PCCP

Accepted Manuscript

ROYAL SOCIETY OF CHEMISTRY

www.rsc.org/pccp

Structural phase transformation and microwave dielectric studies on $SmNb_{1-x}(Si_{1/2}Mo_{1/2})_xO_4$ compounds with fergusonite structure

S.D. Ramarao and V.R.K. Murthy*

Microwave Laboratory, Department of Physics, Indian Institute of Technology Madras,
Chennai 600 036, India.

Abstract:

Temperature and composition induced phase transition in $SmNbO_4$ composition was studied with help of Differential Scanning Calorimetry, Raman spectroscopy and high temperature powder X-ray diffraction measurements. In-situ X-ray diffraction studies reveal that, $SmNbO_4$ possesses monoclinic fergusonite crystal structure at ambient temperature and transform to tetragonal scheelite structure above the transition temperature ($T_o \geq 800\ ^oC$). Second order nature of this transition was confirmed by observing a linear relationship between spontaneous strain (e_s) of $SmNbO_4$ and Landau order parameter (η) in the vicinity of phase transition temperature. With substitution of Si^{4+} and Mo^{6+} in Nb-site of $SmNbO_4$, we have stabilized this high temperature tetragonal scheelite phase at ambient temperature. All the $SmNb_{1-x}(Si_{1/2}Mo_{1/2})_xO_4$ (x = 0.0 – 0.69) ceramic compositions were prepared by conventional solid-state reaction method. Rietveld refinement was carried out on all these compositions to examine the phase purity and observed to form in monoclinic fergusonite (I2/a space group, Z = 2) structure in $x < 0.06$ compositions. Both the X-ray diffraction and Raman spectroscopic measurements reveal that, with increasing the concentration of x, the structure is transformed from monoclinic fergusonite to tetragonal scheelite structure ($I4_1/a$ space group, Z = 4) at a critical concentration (x_c). Both the monoclinic and tetragonal phases were co-existed in $0.06 \leq x < x_c$ composition range. Hakki-Colemann and reflection cavity techniques were used to measure the dielectric constant and quality factor of these stabilized phases respectively. Temperature coefficient of resonant frequency was measured using an

invar cavity attached to the programmable hot plate. Well dense samples possess good microwave dielectric properties.

Keywords: Landau theory; order parameter; X-ray diffraction; Raman spectroscopy; dielectric properties

*Corresponding author, e-mail: vrkm@physics.iitm.ac.in

1. Introduction

The compounds with ABO_4 stoichiometry are technologically important materials showing wide variety of interesting applications such as scintillators, Cherenkov detectors, acousto-optic devices, laser host materials etc. Numerous investigations were also reported on ABO_4 type materials for cathode material in solid state fuel cells, photo catalytic and photoluminescent materials.[1-5] These compounds can accommodate different type of crystal structures depending on the ionic radii and their ratio, valence type like I-VII, II-VI, III-V and IV-IV, the coordination number and electronic configuration (filling of d and *f* shells) of B-site cation.[6]

Generally, metal ortho molybdate ($A^{2+}MoO_4$) and ortho tungstate ($A^{2+}WO_4$) compounds posses scheelite structure when A-site is occupied by large bivalent cations (ionic radius > 0.99 Å) such as Ca, Ba, Sr, Pb, and Eu. Whereas the $A^{2+}(Mo, W)O_4$ compounds with smaller bivalent cations (ionic radius < 0.77 Å, Zn, Co, Ni, Mn and Fe) at A-site gives the wolframite crystal structure.[6] Recently from last decade, researchers focused on the microwave dielectric properties of $A^{2+}B^{6+}O_4$ (A: Ca, Sr, Ba, Zn, Ni, Mg and B: Mo, W) ceramic compositions having scheelite and wolframite crystal structures because of flexibility for the substitution of different elements at A- and B-site to obtain optimum microwave dielectric properties.[7-11]

Ewing reported the crystal chemistry of different class of material with niobium and tantalum.[12] On the other hand, pure rare-earth ortho niobate ($RENbO_4$) compositions crystallize in monoclinic fergusonite crystal structure (I2/a, C_{2v}^{6}) at room temperature and transform to tetragonal scheelite structure after reaching a critical temperature and this temperature depends on the constituent ions in these compositions.[13] Rooksby *et al.* reported this monoclinic fergusonite structure as distorted scheelite structure. This distortion induced due to the presence of micro strains in these compositions. One of the strains causes the unit cell edges unequal and other to the deviation of monoclinic angle from 90°.[14] Therefore, structure changes from monoclinic fergusonite to tetragonal scheelite structure. Researchers predicted that, this monoclinic distortion in fergusonite type compositions might disappear by giving sufficient thermal energy and transform to tetragonal scheelite structure.[13] This type of phase transition was reported by Stubican in rare-earth ortho niobates and tantalates with $A^{3+}B^{5+}O_4$ stoichiometry. Out of these, rare-earth tantalates reported to possess higher transition temperature in comparison with niobates.[13] Rooksby *et al.* reported that the variation in nature of bonding in NbO_4 and TaO_4 tetrahedron was responsible for the difference in the phase transition temperature. Ta – O bonds were more covalent than Nb – O bonds in these compositions and hence, tantalates require more energy to remove this monoclinic distortion.[14] Therefore, this phase transition temperature was sensitive with respect of ionic radius of constituent ions (both rear-earth and B-site cation). Nature of this monoclinic ⇔ tetragonal phase transition is a second-order and displacive.[15] Errandonea *et al.* reported pressure induced scheelite to fergusonite structural transformation in $CaWO_4$ and $SrWO_4$ compositions using angle dispersive X-ray diffraction and near edge X-ray absorption studies.[16]

High temperature tetragonal phase of $LaNbO_4$ was stabilized by substitution of lower ionic radius V^{5+} (0.355 Å) in the place of Nb^{5+} (0.48 Å).[17,18] In the same report author explained the variation in lattice parameters a, c and monoclinic angle β with increasing the V^{5+} concentration. Similar variation in the lattice parameters was reported by Aldred in $CeNbO_4$ and $NdNbO_4$ compositions. Nature of phase transition in $RENbO_4$ (Re: La, Ce and Nd) composition was explained by Aldred with help of landau theory.[19] One of the most important conclusions from the same report by Aldred was, V^{5+} substitution in place of Nb^{5+} cannot be stabilized the high temperature tetragonal scheelite structure of $RENbO_4$ compositions with heavier rare- earth ion at A-site of these compositions.[19]

This triggered us to investigate the phase transition mechanism and its stabilization studies on the $SmNbO_4$ composition. To our knowledge there are no any experimental reports on the phase transition mechanism and composition induced structural transition in $SmNbO_4$ composition. Therefore, in the present manuscript, we report the nature of the phase transition and stabilization of high temperature crystal structure of $SmNbO_4$ with substitution of multiple cations (Si^{4+} and Mo^{6+}) at Nb-site. We report the microwave dielectric properties of both monoclinic and stabilized tetragonal phases.

2. Experimental procedure

$SmNb_{1-x}(Si_{1/2}Mo_{1/2})_xO_4$ (x = 0.0 – 0.69) ceramic compositions were synthesized by conventional solid-state reaction method. The proportionate amounts of initial ingredients Sm_2O_3 (99.9%), Nb_2O_5 (99.5 %), SiO_2 (99.8 %) and MoO_3 (99.95 %) were collected in a mortar and ground using pestle. Both wet and dry mixing procedures were followed to achieve homogeneous mixtures. Moisture sensitive rare-earth oxide (i.e. Sm_2O_3) was pre-heated at 800 °C for 10 h before weighing in stoichiometry ratio. All the grounded homogeneous mixtures were collected in to high pure alumina crucibles and are calcined in the temperature range 1200 – 1300 ^{o}C for 4 h. The agglomerated product obtained after calcination procedure were made in to fine powder by following both the dry and wet grinding. Phase purity of $SmNb_{1-x}(Si_{1/2}Mo_{1/2})_xO_4$ ($x = 0.0 – 0.69$) compositions were studied by collecting the powder X-ray diffractograms of these compositions using Philips PANAlytical X'pert Pro X ray diffractometer with X'Celerator detector. We have used Cu K_{α} radiation with an accelerating voltage 40 kV and 30 mA current. The incident and receiving soller slits were maintained with 0.02° whereas 1° divergent slit was use for all these measurements. The data was collect with a step of 0.017°. In order to understand the structural transformation, we have done Rietveld refinement on all these compositions following the procedure given in the notes of Canadian Powder Diffraction Workshop.[20] The pseudo-voigt function was used to fit the peak shape using GSAS suite with EXPGUI software.[21,22]

Room temperature Raman spectra of these samples were obtained by using Horiba Jobin Yvon HR800 UV Raman spectrometer equipped with Peltier-cooled charge-coupled device detector. He-Ne laser source ($\lambda = 632.8$ nm) is used for the measurement and the laser output power measured at the sample is about 3 mW. Polished (using 0.25 μm diamond paste) and thermally etched (heated at 500 ^{o}C for 8 h to remove the strains due to polishing) samples were used for these measurements. The measurement was performed in the backscattering geometry. The incident slit aperture of 100 μm and grating of 1800 lines/inch were used to obtain the resolution of 0.3 cm^{-1}. An Olympus BX-41 microscope with 100× objective lens is used to obtain the laser spot of diameter about 1 μm on the sample. The spectrometer is calibrated with silicon standard prior to the measurement.

Phase stability of $SmNbO_4$ with temperature was probed by Differential Scanning Calorimetry (DSC) and temperature variation XRD measurements using SDT Q600, TA

Instruments and Philips PANAlytical X'pert Pro X-ray diffractometer equipped with high temperature chamber HTK 16N, Anton Paar respectively. By adding 3 wt% poly vinyl alcohol, pellets of 8 mm diameter and 7 mm thickness were prepared out of these calcined powders. Sintering temperature of these compositions was optimized using conventional resistive heating furnace. Archimedes technique was used for measuring the bulk density of these sintered pellets and compared with the theoretical density obtained from Rietveld refinement. Microwave dielectric properties such dielectric constant (ε_r) and quality factor ($Q\times f$) were measured by Hakki-Colemann method and reflection cavity technique respectively. Temperature coefficient of resonant frequency (τ_f) was measured in the temperature range of 25–85^{o}C using an invar cavity attached to programmable hot plate.

3. Results and Discussion

3.1. Temperature induced phase transition in $SmNbO_4$

Differential Scanning Calorimetry (DSC), temperature variation powder X-ray diffraction techniques were used to understand the phase transition mechanism in $SmNbO_4$ composition. In general, DSC is a very important tool for identifying any structural changes in different class of materials by measuring the heat flow of corresponding phase transition. Fig. 1(a) shows the DSC scan of $SmNbO_4$ composition in the temperature range 100 – 1400 ^{o}C. A heating rate 20 ^{o}C/min was used for this measurement. We can clearly seen a transition starting from 650 to 1130 ^{o}C in this Fig. 1(a) and transition temperature of this composition was obtained by differentiating the DSC scan in the range 700 – 900 ^{o}C and found to have transitions at 762 ^{o}C and 789 ^{o}C.

In order to understand the mechanism of these phase transitions, we have done temperature variation powder X-ray diffraction measurements on $SmNbO_4$ composition in the temperature range 30 – 850 °C and are shown in Fig. 1(b). Rietveld refinement analysis was carried out on all these diffractograms and observed to possess monoclinic fergusonite structure at room temperature. Therefore, the room temperature powder X-ray diffractogram of $SmNbO_4$ was indexed with monoclinic space group (I2/a) and JCPDF file no. 32-0496. We have not observed much variation in X-ray reflection of $SmNbO_4$ up to certain temperature. With increasing the temperature, we observed to see changes in X-ray reflections of this composition and onset of the phase transition might be responsible for these variations. Fig. 1 (b) clearly indicates that, with increasing the temperature, the maximum intense reflections (-121) and (031) of room temperature $SmNbO_4$ composition approach toward each other whereas (040) and (002) reflections deviated from each other. Rietveld refinement reveals that the high temperature phase of $SmNbO_4$ was well fitted with the tetragonal scheelite structure with $I4_1/a$ space group and resulting satisfactory refinement parameters ($_wR_p$, R_p and χ^2). Hence, high temperature powder X-ray diffractogram of $SmNbO_4$ was indexed with tetragonal space group. The Rietveld refinement plots of $SmNbO_4$ at ambient and transition temperature are shown in Fig. 2(a). Crystal structure of $SmNbO_4$ at room temperature and high temperature are shown in Fig. 2(a). Crystallographic information like space group, atomic positions, bond lengths and occupancies of both the room temperature and high temperature phases are given in the Table 1.

Arrangement of B-site tetrahedron is one of the important differences between room temperature fergusonite and high temperature scheelite structure of $SmNbO_4$ composition and is shown in Fig. 2(b). This Fig. depicts that, B-site tetrahedron are distorted along one of its diagonals in room temperature Fergusonite structure which is because of the strains present in the $SmNbO_4$ composition. On the other hand, symmetrical isolated B-site tetrahedral arrangement is seen in high temperature scheelite structure because of decrease in the strains with increasing the temperature and is confirmed by calculating the spontaneous strain of $SmNbO_4$. Fergusonite structure observed to possess two distinguishable oxygen positions O(1) and O(2) whereas the high temperature scheelite structure of $SmNbO_4$ contains only one oxygen position in the unit cell. In high temperature scheelite structure A-site Sm^{3+} cation is connected with eight oxygen forming SmO_8 dodecahedron whereas in the case of room temperature $SmNbO_4$ structure, two oxygen O(1) and O(2) are connected with A-site Sm^{3+} cations with two sets of shorter and longer bonds.

The variation in the lattice parameters (a_M, b_M, c_M, a_T and c_T) and β of $SmNbO_4$ composition with increasing the temperature is shown in Fig. 3(a) and 3(b) respectively. The suffix M corresponds to room temperature monoclinic fergusonite structure whereas the suffix T belongs to tetragonal scheelite structure. From this Fig. 3(a) we can clearly understand that, with increasing the temperature, the parameters b_M and c_M are observed to increase whereas a_M and β are decreased with increasing the temperature. On reaching the phase transition temperature (T_o), the lattice parameters a_M and c_M corresponding to monoclinic phase became equal whereas the monoclinic angle β approached to 90°. Therefore, these changes in the lattice parameters result the decrease of monoclinic distortion in $SmNbO_4$ compound and transform the symmetry of the structure from monoclinic to tetragonal. Table 2 gives the lattice parameters of $SmNbO_4$ composition at different temperatures.

Monoclinic distortion in $SmNbO_4$ is arising due to presence of two homogeneous strains. One of the strain, $(e_1 - e_2)$ transforms the square base of the tetrahedron in tetragonal structure to parallelepiped in monoclinic structure. Another strain, e_6 deviate the angle β from 90°. In the present studies we have calculated these strains in $SmNbO_4$ using the following expressions and the lattice parameters obtained from Rietveld refinement on temperature variation diffractograms of $SmNbO_4$ and are given in Table 3.[19]

$$(e_1 - e_2) = \frac{(a_M - c_M)}{(a_M c_M)^{1/2}} \quad \text{and} \quad e_6 = \cos(\pi - \beta) \qquad (1)$$

Where, a_M, c_M and β are the lattice parameters of monoclinic $SmNbO_4$ whereas e_1, e_2 and e_6 represents the elements of strain tensor.

The variation in both these homogeneous strains with increasing temperature is shown in Fig. 3(c). This clearly depicts that, both $(e_1 - e_2)$ and e_6 strains observed to decrease with increasing the temperature and become zero when the system reaches the transition temperature (T_o ~ 800 ^oC). The decrease in $(e_1 - e_2)$ is responsible for the lattice parameters a_M and c_M to become equal whereas the variation in monoclinic angle with temperature is attributed to the decrease of e_6 strain in $SmNbO_4$. This confirms that, the monoclinic distortion vanishes with increase in temperature. In addition to these, we have calculated evolution of basal area of tetrahedron ($A_M^{1/2}$, $A_T^{1/2}$) and unit cell volume ($V_M^{1/3}$, $V_T^{1/3}$) with temperature and are shown in Fig. 3(c). The suffix M and T represents the monoclinic and tetragonal phases respectively. This shows a clear discontinuity in volume and basal area at the phase transition temperature (T_o ~ 800 ^oC). Transition temperature obtained from both DSC and high temperature powder X-ray diffraction measurements is in good agreement. We observed a slight variation in the transition temperature in comparison with the theoretical value and this could be attributed to the synthesis conditions.[23,24] Errandonea *et al.* reported the pressure driven phase transitions in the $A^{2+}WO_4$ (A: Ca, Sr, Ba, Eu and Pb) compositions and explained the phase transition mechanism with the help of Landau theory of phase transitions.[25] As there are no experimental reports on the phase transitions mechanism of

$SmNbO_4$ ceramic compositions, we explain this behaviour with help of Landau theory of phase transitions.

Two homogeneous strains are responsible for tetragonal to monoclinic phase transformation and leads to the formation of two possible orientation states (S_1 and S_2) in monoclinic fergusonite structure. Presence of these strains influence the crystal symmetry and hence changes from 4/m to 2/m. The distortion of each orientation is described with help of second rank strain tensor for monoclinic symmetry gives as follows[25]

$$e_{ij}\left(S_1\right)=\begin{pmatrix} e_{11} & e_{12} & e_{13} \\ e_{21} & e_{22} & 0 \\ 0 & 0 & e_{33} \end{pmatrix} \tag{2}$$

Here, S_1 is the one orientation state and other orientation state S_2 can be obtained by $e_{ij}\left(S_2\right)=\mathrm{R}\, e_{ij}(S_1)\mathrm{R}^{\mathrm{T}}$ equation where R and R^{T} represents the 90^{o} rotation matrix around monoclinic b-axis and it's transpose. Strain components for the present monoclinic to tetragonal transition were calculated using the lattice parameters obtained from Rietveld refinement and following expressions.[18,26]

$$e_{11}=\frac{c_M \sin\beta_M}{a_T}-1 \tag{3a}$$

$$e_{22}=\frac{a_M}{a_T}-1 \tag{3b}$$

$$e_{33}=\frac{b_M}{c_T}-1 \tag{3c}$$

$$e_{12}=\frac{1}{2}\frac{c_M \cos\beta_M}{a_T} \tag{3d}$$

Where, the lattice parameters corresponding to monoclinic symmetry are represented as a_M, b_M, c_M and for tetragonal symmetry as a_T, c_T and β_M. Here, suffixes M and T correspond to monoclinic and tetragonal crystal systems. We have calculated both the longitudinal and shear strains using the following equations derived by Aizu for monoclinic to tetragonal transition.[27]

$$e_{ij}^{s}\left(S_1\right)=\begin{pmatrix} -u & v & 0 \\ v & u & 0 \\ 0 & 0 & 0 \end{pmatrix} \tag{4a}$$

$$e_{ij}^{s}\left(S_2\right)=\begin{pmatrix} u & -v & 0 \\ -v & -u & 0 \\ 0 & 0 & 0 \end{pmatrix} \tag{4b}$$

where $u=\frac{1}{2}\left(e_{22}-e_{11}\right)$ is longitudinal strain

and $v=e_{12}$ is shear strain

The scalar spontaneous strain for monoclinic to tetragonal transition in $SmNbO_4$ was calculated with increasing temperature using the following expression and is given in Table 4.

$$e_s=\sqrt{u^2+v^2} \qquad 4(c)$$

Vullam *et al.* explained the phase transition mechanism in $LaNbO_4$ with help of Landau theory and concluded that, the transition was second order in nature and follows a linear relation between order parameter (η) and the spontaneous strain (e_s). Where, the order parameter (η) was defined as follows.[15]

$$\eta = \left(\frac{T_o - T}{T}\right)^{1/2} \quad \text{and} \quad \eta = ke_s \qquad (5)$$

Here, T_o represents the phase transition temperature and k is correlation number which is a constant for all the temperatures and specific for a particular system under study.

Fig. 4 shows relation between order parameter divided by k (i.e. η/k) and the spontaneous strain (solid spheres) values of $SmNbO_4$ composition. We have optimized the value of k (10.25) for getting better fitting with the obtained data points. We could not obtain proper fit at lower temperatures. But, when we are moving toward the phase transition temperature, a linear variation between the order parameter and spontaneous strain values was observed and this confirms that the phase transition in $SmNbO_4$ is second order in nature.

3.2. Composition induced structural transformation in $SmNbO_4$: X-ray diffraction and Raman spectroscopic studies

Room temperature X-ray diffractograms of $SmNb_{1-x}(Si_{1/2}Mo_{1/2})_xO_4$ (x = 0.0 – 0.69) compositions are shown in Fig. 5(a). We have done Rietveld refinement on all these compositions and observed to possess monoclinic symmetry in $x < 0.06$ compositions and these diffractograms are indexed with monoclinic fergusonite structure with I2/a space group. With further increasing the concentration of x, the intensity of the reflections (-121) and (031) corresponding to monoclinic fergusonite structure observed to decrease and an additional reflection is started in between these reflections. Rietveld refinement on these compositions reveals that both monoclinic fergusonite and tetragonal scheelite structures are coexisted in $0.06 < x \leq 0.68$ composition range. $SmNb_{1-x}(Si_{1/2}Mo_{1/2})_xO_4$ composition with $x = 0.69$ observed form in tetragonal scheelite structure with $I4_1/a$ space group which is the high temperature crystal structure of $SmNbO_4$ compositions. Hence, with substitution of Si^{4+} and

Mo^{6+} ions in place of Nb^{5+}, we have stabilized the high temperature crystal structure of $SmNbO_4$ composition. The crystallographic information like atomic positions and occupancies are given in Table 5 and the corresponding refinement plot is shown in Fig. 5(b).

Fig. 5(c) shows the variation in lattice parameters of $SmNb_{1-x}(Si_{1/2}Mo_{1/2})_xO_4$ ($x = 0.0 - 0.69$) compositions. It is clearly depict from this Fig. that, in the solid solution region (i.e. $x < 0.06$), we have not seen much variation in lattice parameters. With further increasing the concentration of x, the lattice parameters a_M and c_M corresponding to monoclinic structure became equal whereas the b_M value increased to 11.38 Å in tetragonal structure. Similarly, the monoclinic angle β decreased from 94.75^o to 90^o. In order to understand clearly, different crystallographic phase regions are given in Fig. 5c similar to earlier reports by Zhou *et al.*[27,28] In $ANb_{1-x}V_xO_4$ (A: Ce, Nd; $x = 0.0 - 1.0$) system, Aldred observed solid solution up to $x \leq 0.30$ where the lattice parameters corresponding to monoclinic structure became equal and observed an increase in the b_M value.

Aldred explained the composition induced phase transition mechanism in $ANb_{1-x}V_xO_4$ (A: Ce, Nd; $x = 0.0 - 1.0$) compositions with help of Landau theory.[19] Aldred calculated the strain parameters using the lattice parameters and explained second order nature of this phase transition. Formation of very less solid solution region (i.e. $x < 0.06$) in our present study on $SmNb_{1-x}(Si_{1/2}Mo_{1/2})_xO_4$ compositions restricted us to get more number of data points (lattice and strain parameters) to understand the exact phase transition mechanism in these compositions. As the lattice parameter variation in $SmNb_{1-x}(Si_{1/2}Mo_{1/2})_xO_4$ ($x = 0.0 - 1.0$) compositions is analogous to the variation in $ANb_{1-x}V_xO_4$ (A: Ce, Nd; $x = 0.0 - 1.0$) system reported by Aldred, decreasing the monoclinic distortion with increasing the concentration of Si^{4+} and Mo^{6+} might be responsible for this monoclinic to tetragonal transition in $SmNbO_4$ composition.

Raman spectroscopy is very important spectroscopic technique to understand the local environment (ordered or disordered) and gives more information about any structural changes in different class of materials. In the present study, in order to understand the effect of substitution of Si^{4+} and Mo^{6+} at Nb^{5+} site of $SmNbO_4$ composition on the vibrational characteristics, we have done room temperature Raman spectroscopic measurements on $SmNb_{1-x}(Si_{1/2}Mo_{1/2})_xO_4$ ($x = 0.0 – 0.69$) compositions. Fig. 6 shows the Raman spectra of all these compositions in 25 – 1100 cm^{-1} range. It is well known that at room temperature $SmNbO_4$ composition observed to possess monoclinic crystal symmetry with I2/a space group. In this structure both Sm^{3+} and Nb^{5+} cations occupy 4e Wyckoff site whereas oxygen anions occupy 8f site.[29] Group theoretical analysis predicts that there are 18 Raman active modes possible for monoclinic Fergusonite structure and irreducible representation of these modes is given below.[29,30]

$$\Gamma = 8A_g+10B_g+8A_u+10B_u$$

Where all the ‘g’ vibrations are Raman active and all ‘u’ modes are IR active.

In the present studies, the obtained Raman spectra are in good agreement with the earlier reports[29] and all the modes were assigned and are shown in Fig. 6. Raman modes of fergusonite structure are grouped into external and internal modes considering RE^{3+} and NbO_4 as two sub-lattices where the modes corresponding to the vibrations of NbO_4 are appear at high wavenumber side because of covalence nature of Nb – O bonds. On the other hand, all the external modes are present in low wavenumber side. In the compositions with $x < 0.06$, we have not seen any shift in the Raman modes of $SmNbO_4$ whereas an increase in the full width at half maxima (FWHM) of the intense Raman modes (A_g at 808.7 cm^{-1}, 331.4 cm^{-1} and 120.3 cm^{-1}) was observed. As the A_g modes are arising from the symmetrical stretching vibrations (ν_{sys}) of Nb – O bonds, substitution of Si^{4+} and Mo^{6+} ions at Nb^{5+} site influences the rigidity of the NbO_4 tetrahedra and is reflecting in the FWHM of A_g modes.

A new Raman active mode around 868.8 cm^{-1} is observed to start from x = 0.06 composition. Powder X-ray diffraction measurements on $SmNb_{1-x}(Si_{1/2}Mo_{1/2})_xO_4$ (x = 0.69) compositions confirm that the tetragonal phase is started from x = 0.06 composition and single phase tetragonal scheelite structure was observed for x = 0.69 composition. With this information, we can confidently assign this new mode at 884.4 cm^{-1} in x = 0.69 composition to Ag mode which is the highest intense mode corresponding to symmetric stretching vibrations of (Nb/Si/Mo) – O bonds in the tetragonal scheelite structure. The mode at 814.4 cm^{-1} is assigned to the asymmetric stretching vibrations of (ν_{asy}) of (Nb/Si/Mo) – O bonds and complete assignment of Raman modes for x = 0.69 compositions with tetragonal Scheelite structure is shown in Fig. 6(a). For clear understanding, we have deconvoluted the Raman spectrum of x = 0.69 composition and is shown in Fig. 6(b). This Fig. clearly indicate that the symmetrical stretching vibrational mode corresponding to tetragonal scheelite structure shifts towards high wavenumber side and can be attributed to the substitution of lower ionic radius Si^{4+} (0.26 Å) and Mo^{6+} (0.41 Å) in place of Nb^{5+} (0.48 Å)[17] which inturn influences the covalence of (Nb/Si/Mo) – O bonds. The low wavenumber Raman modes of $SmNb_{1-x}(Si_{1/2}Mo_{1/2})_xO_4$ (x = 0.69) composition with scheelite structure are weak in their intensity in comparison the x = 0 composition with fergusonite structure. Presence of multiple cations at B-site might be responsible for this type of behaviour. In the present study we could assign some of the Raman modes of $SmNb_{0.31}(Si_{1/2}Mo_{1/2})_{0.69}O_4$ compound with tetragonal scheelite structure and are given in Table 6. Along with powder X-ray diffraction analysis, this systematic variation in the Raman spectra of $SmNb_{1-x}(Si_{1/2}Mo_{1/2})_xO_4$ (x = 0.0 –

0.69) compositions confirms the transformation of monoclinic Fergusonite to tetragonal Scheelite structure with substitution of Si^{4+} and Mo^{6+} in place of Nb^{5+}.

As this phase transition temperature is sensitive to the ionic radius of the constituent elements, in order to observed the effect of substitution of Si^{4+} and Mo^{6+} at Nb site of $SmNbO_4$, we have done DSC measurements on $SmNb_{1-x}(Si_{1/2}Mo_{1/2})_xO_4$ (x = 0.0, 0.03, 0.04) compositions. Fig. 7 shows the DSC scans of these compositions and from this we can clearly seen that the phase transition temperature (T_o) is increased slightly with increasing concentration of x. Substitution of lower ionic radius elements (Si^{4+} and Mo^{6+}) in place of higher ionic radius element (Nb^{5+}) increases the covalence of the corresponding bonds and needs higher energy to remove monoclinic distortion in these compositions. Hence, variation in the covalence might be responsible for increase in this phase transition temperature. Increase in the phase transition temperature is less because of substitution of lower concentration of Si^{4+} and Mo^{6+} in place of Nb^{5+}. These DSC measurements reveal that the unknown phase transition around 760 °C is suppressed with increasing the concentration of x. We are unable to understand the exact reason for suppression of this unknown phase transition.

4. Density and Microstructural studies

Archimedes principle was used to measure the bulk density of sintered pellets of $SmNb_{1-x}(Si_{1/2}Mo_{1/2})_xO_4$ (x = 0.0 – 0.69) compositions. The percentage density was calculated using both the measured and theoretical density of respective compositions. The theoretical density of all these compositions was calculated using the following formula.[31]

$$\rho_{th} = \frac{nM}{NV} \text{ g.cm}^{-3} \tag{3.2}$$

Where, n and M represents the number of formula units per unit cell which can be obtained from the crystal structure of respective composition and molecular weight respectively. N is the Avogadro's number (6.022×10^{23} mol^{-1}) and V is the molar volume of the corresponding composition and is calculated using lattice parameters obtained from Rietveld refinement. Percentage of theoretical density of all these compositions was calculated using the following equation.

$$\rho(\%) = \frac{\rho_m}{\rho_{th}} \times 100$$

Where, ρ_m = measured density and ρ_{th} = theoretical density

All $SmNb_{1-x}(Si_{1/2}Mo_{1/2})_xO_4$ (x = 0.0 – 0.69) compositions observed to possess more than 95% theoretical density. Scanning Electron Microscope (FEI quanta 400 high resolution Scanning Electron Microscope) studies on polished and thermally etched compositions reveal that (Fig. 8), the microstructures are well compacted and not much variation in grain size was observed with substitution of Si^{4+} and Mo^{6+} in place of Nb^{5+} of $SmNbO_4$.

5. Microwave dielectric studies on $SmNb_{1-x}(Si_{1/2}Mo_{1/2})_xO_4$ (x = 0.0, 0.03, 0.04, 0.68 and 0.69) compositions

Microwave dielectric properties such as dielectric constant and quality factor of $SmNb_{1-x}(Si_{1/2}Mo_{1/2})_xO_4$ (x = 0.0, 0.03, 0.04, 0.68 and 0.69) ceramic compositions were measured using Hakki-Colemann and reflection cavity techniques respectively whereas temperature coefficient of resonant frequency of these compositions was measured with help of an invar cavity attached to programmable hot plate. Microwave dielectric properties of all these compositions are given in Table 7.

The variation in dielectric constant of $SmNb_{1-x}(Si_{1/2}Mo_{1/2})_xO_4$ (x = 0.0, 0.03, 0.04, 0.68 and 0.69) compositions is shown in Fig. 9. In general, dielectric constant of ceramic materials depends on the extrinsic parameters such as porosity, secondary phases and intrinsic parameters like polarizability and structural characteristics of materials.[32-34] In our present studies, $SmNb_{1-x}(Si_{1/2}Mo_{1/2})_xO_4$ (x = 0.0, 0.03, 0.04, 0.68 and 0.69) compositions possess more than 95% theoretical density and hence, effect of porosity on dielectric constant of these materials is negligible. Choi *et al.* reported that the dielectric constant of ceramic materials at microwave frequencies depends on the ionic polarizability of constituent ions.[35] In a similar way, Kim *et al.* explained the higher dielectric constant of lead based scheelite structured materials than ABO_4 (A: Ca, Ba; B: Mo, W) compounds with its higher ionic polarizability than other ions.[36] In our present studies, the dielectric constant is observed to decrease with increasing the concentration of x. In literature it was reported that Si^{4+} (0.87 $Å^3$) and Mo^{6+} (3.60 $Å^3$) possess lower polarizability than Nb^{5+} (3.97 $Å^3$).[37] Therefore, with increasing the concentration of x, as we are replacing the higher polarizable Nb^{5+} (3.97 $Å^3$) ion with lower polarizable Si^{4+} (0.87 $Å^3$) and Mo^{6+} (3.60 $Å^3$) ions. Hence, decrease in the dielectric constant of $SmNb_{1-x}(Si_{1/2}Mo_{1/2})_xO_4$ (x = 0.0, 0.03, 0.04, 0.68 and 0.69) compositions is explained with the lower polarizability of Si^{4+} (0.87 $Å^3$) and Mo^{6+} (3.60 $Å^3$) ions.

Quality factor of $SmNb_{1-x}(Si_{1/2}Mo_{1/2})_xO_4$ (x = 0.0, 0.03, 0.04, 0.68 and 0.69) compositions was measured using reflection cavity technique and are given in Table 7. Fig. 10 shows the quality factor variation with increasing the concentration of x. Pure rare-earth ortho niobate compound ($SmNbO_4$: 48200 GHz) with monoclinic fergusonite structure possess higher quality factor than the stabilized (x = 0.69: 32800 GHz) composition with tetragonal scheelite structure. Quality factor of ceramic materials at microwave frequencies depends on processing parameters such as density, porosity, secondary phases and grain growth.[38,39] Surendran *et al.* reported the dependence of quality factor on structural transitions in microwave dielectric materials where they observed to see decrement in quality factor when moving towards the phase transition region.[40] In a similar way, Solomon *et al.* explained the decrease in quality factor with phase transition mechanism.[41] In our present studies on $SmNb_{1-x}(Si_{1/2}Mo_{1/2})_xO_4$ when we are moving from the $x = 0.0$ to 0.69, the structure is continuously changing from the monoclinic to tetragonal which is confirmed by both X-ray and Raman spectroscopic measurements. This onset of structural changes might be responsible for the systematic decrement in the quality factor which is clearly shown in Fig. 10.

Fig. 10 shows the variation in temperature coefficient of resonant frequency (τ_f) of $SmNb_{1-x}(Si_{1/2}Mo_{1/2})_xO_4$ (x = 0.0, 0.03, 0.04, 0.68 and 0.69) ceramic compositions. When we are moving from Nb^{5+} rich to Nb^{5+} poor compositions, τ_f is observed to change from -47 ppm/°C for $x = 0.0$ to -38 ppm/°C for $x = 0.69$ composition. Therefore, we observed a slight improvement in τ_f and shifting toward zero value when the systems approaching the phase transition region which is in consistence with the earlier reports on microwave dielectric materials where they reported that temperature coefficient of resonant frequency (τ_f) is reported to have minimum values when the system is approaching the phase transition region.[42]

6. Conclusions

All the $SmNb_{1-x}(Si_{1/2}Mo_{1/2})_xO_4$ (x = 0.0 – 0.69) compositions were synthesized by solid state reaction method. Temperature variation X-ray diffraction measurements reveal that pure rare-earth ortho niobate ($SmNbO_4$) possess monoclinic fergusonite structure with

I2/a space group at room temperature and transform to tetragonal scheelite structure with $I4_1/a$ around 800 °C. Nature of this transition was explained with Landau theory. Both room temperature powder X-ray diffraction and Raman spectroscopic measurements on $SmNb_{1-x}(Si_{1/2}Mo_{1/2})_xO_4$ compositions reveal that the crystal system moving form monoclinic to tetragonal with increasing the concentration of x. Rietveld refinement reveals that $SmNb_{1-x}(Si_{1/2}Mo_{1/2})_xO_4$ form a solid solution up to $x < 0.06$ with monoclinic fergusonite structure whereas the composition $x = 0.69$ form in the tetragonal scheelite structure. Both monoclinic and tetragonal phases were coexisted in $0.06 < x \leq 0.68$ ranges and similar variation was observed even in Raman spectroscopic measurements. Unknown transition around 760 °C was suppressed with substitution of Si^{4+} and Mo^{5+} in place of Nb^{5+}. Moreover, a slight increment in phase transition temperature (T_o) was observed with increasing the concentration of x from 0.0 to 0.04. Both the monoclinic and stabilized tetragonal phases possess good microwave dielectric properties.

Acknowledgement

Author S.D. Ramarao thanks University Grants Commission, Delhi, India and Indian Institute of Technology Madras for providing fellowship in the form of Senior Research Fellowship.

References:

1. I.A. Kamenskikha, V.N. Kolobanova, V.V. Mikhailina, L.I. Potkinc, I.N. Shpinkova, D.A. Spasskya, B.I. Zadneprovskyc and G. Zimmerer, *Nucl. Instrum. Methods. Phys. Res. Sect. A.* 2001, **470**, 270.
2. L. Hoffart, U. Heider, L. Jorissen, R.A. Huggins and W. Witschel, *Ionics.* 1995, **1**, 131.
3. B. Yan and J.H. Wu, *Mater. Chem. Phys.* 2009, **116**, 67.
4. H. Shi, X. L. Huang, H. Tian, J. Lv, Z. Li, J. Ye and Z. Zou, *J. Phys. D: Appl. Phys.* 2009, **42**, 125402.
5. D.A. Pinnow, L. G. Van Uitert, A. W. Warner and W. A. Bonner, *Appl. Phys. Letters.* 1968, **15**, 83.
6. K.S. Vorres, *J. Chem. Educ.* 1962, **39**, 566.
7. S.H. Yoon, D.W. Kim, S.Y. Cho and K.S. Hong, *J. Eur. Ceram. Soc.* 2006, **26**, 2051.
8. R.C. Pullar, S. Farrah and N.M. Alford, *J. Eur. Ceram. Soc.* 2007, **27**, 1059.
9. E.S. Kim, B.S. Chun, R. Freer and R.J. Cernik, *J. Eur. Ceram. Soc.* 2010, **30**, 1731.
10. G.K. Choi, J.R. Kim, S.H. Yoon and K.S. Hong, *J. Eur. Ceram. Soc.* 2007, **27**, 3063.
11. D. Zhou, L.-X. Pang and Z.-M. Qi, *Inorg. Chem.* 2014, **53**, 9222.
12. R.C. Ewing, *American Mineralogist.* 1975, **60**, 728.
13. V.S. Stubican, *J. Am. Ceram. Soc.* 1964, **47**, 55.
14. H.P. Rooksby and E.A.D. White, *Acta Cryst.* 1963, **16**, 888.
15. F. Vullum, F. Nitsche, S.M. Selbach and T. Grande, *J. Solid State Chem.* 2008, **181**, 2580.
16. D. Errandonea, J.P. Porres, F.J. Manjon, A. Segura, Ch. F. Roca, R.S. Kumar, O. Tschauner, P.R. Hernandez, J.L. Solano, S. Radescu, A. Mujica, A. Munoz and G. Aquilanti, *Phys. Rev. B.* 2005, **72**, 174106.
17. R.D. Shannon, *Acta Crystallogr. A.* 1976, **32**, 751.

18. A.T. Aldred, *Mater. Lett.* 1983, **1**, 197.

19. A.T. Aldred, *J. Solid State Chem.* 1985, **59**, 95.

20. L. Cranswick and I. Swainson, 7th Canadian Powder workshop notes: http:/www.cins.ca/cpdw/notes.html. 2007.

21. A.C. Larson and R.B. von Dreele, General Structural Anal-ysis System (GSAS), Los Alamos National Laboratories, Los Alamos, NM, 1990.

22. B.H. Toby, *J. Appl. Crystallogr.* 2001, **34**, 210.

23. E.K. Salje, Phase Transitions in Ferroelastic and Co-elastic Crystals, Cambridge University Press, 1991.

24. K. Ishikawa, K. Yoshikawa and N. Okada, *Phys. Rev. B.* 1988, **37**, 5852.

25. D. Errandonea, *Europhys. Lett.* 2001, **77**, 56001-P1.

26. J.L. Schlenker, G.V. Gibbs and M.B. Boisen, *Acta Crystallogr. A.* 1978, **34**, 52.

27. D. Zhou, L.-X. Pang, J. Guo, Z.-M. Qi, T. Shao, X. Yao and C.A. Randall, *J. Mater. Chem.* 2012, **22**, 21412.

28. D. Zhou, W.-B. Li, L.-X. Pang, J. Guo, Z.-M. Qi, T. Shao, X. Yao and C.A. Randall, *Dalton Trans.* 2014, **43**, 7290.

29. K. Aizu, *J. Phys. Soc. Jpn.* 1970, **28**, 706.

30. K.P.F. Siqueira, L.R. Moreira and A. Dias, *Chem. Mater.* 2010, **22**, 2668.

31. D.L. Rousseau, R.P. Bauman and S.P.S. Porto, *J. Raman Spectrosc.* 1981, **10**, 253.

32. Q. Liao, L. Li, X. Ren and X. Ding, *J. Am. Ceram. Soc.* 2011, **94**, 3237.

33. S.J. Penn, N. Mc N. Alford, A. Templeton, X. Wang, M. Xu, M. Reece and K.J. Scherapel, *J. Am. Ceram. Soc.* 1997, **80**, 1885.

34. W.S. Kim, E.S. Kim and K.H. Yoon, *J. Am. Ceram. Soc.* 1999, **82**, 2111.

35. A. Dias, G. Subodh, M.T. Sebastian, M.M. Lage and R.L. Moreira, *Chem. Mater.* 2008, **20**, 4347.

36. G.K. Choi, J.R. Kim, S.H. Yoon and K.S. Hong, *J. Eur. Ceram. Soc.* 2007, **27**, 3063.
37. E.S. Kim, B.S. Chun, R. Freer and R.J. Cernik, *J. Eur. Ceram. Soc.* 2010, 30, 1731.
38. R.D. Shannon, *J. Appl. Phys.* 1993, **73**, 348.
39. M.H. Liang, C.T. Hu, H.F. Cheng, I.N. Lin and J.J. Steeds, *J. Eur. Ceram Soc.* 2001, **21**, 2759.
40. W.S. Kim, E.S. Kim and K.H. Yoon, *J. Am. Ceram. Soc.* 1999, **82**, 2111.
41. K.P. Surendran, P. Mohanan and M.T. Sebastian, *J. Eur. Ceram. Soc.* 2003, **23**, 2489.
42. S. Solomon, M. Kumar, K.P. Surendran, M.T. Sebastian and P. Mohanan, *Mater. Chem. Phys.* 2001, **67**, 291.

Table captions:

Table 1 Crystallographic parameters of ambient and high temperature structures of $SmNbO_4$ compound

Table 2 Temperature variation lattice parameters (a, b, c and β) of $SmNbO_4$

Table 3 Temperature variation strain parameters ($(e_1 - e_2)^2, e_6^2$), basal area ($A^{1/2}$) and volume ($V^{1/3}$) of $SmNbO_4$ compound

Table 4 Spontaneous strain values of $SmNbO_4$

Table 5 Wyckoff sites, atomic coordinates and occupancies of $SmNb_{0.31}(Si_{1/2}Mo_{1/2})_{0.69}O_4$ composition

Table 6 Raman mode assignment for $SmNb_{0.31}(Si_{1/2}Mo_{1/2})_{0.69}O_4$ composition

Table 7 Lattice parameters, Percentage of theoretical density (ρ %) and microwave dielectric properties (dielectric constant (ε_r), quality factor ($Q\times f$) and temperature coefficient of resonant frequency (τ_f)) of $SmNb_{1-x}(Si_{1/2}Mo_{1/2})_xO_4$ compositions

Fig. captions:

Fig. 1(a) Differential Scanning Calorimetry Scan of $SmNbO_4$ compound

Fig. 1(b) Temperature variation X-ray diffractograms of $SmNbO_4$

Fig. 2 (a) Rietveld refinement plots and crystal structure of $SmNbO_4$ at 30 ^{o}C and 800 ^{o}C

Fig. 2(b) Tetrahedral arrangement in (i) room temperature monoclinic Fergusonite (ii) high temperature tetragonal Scheelite structure

Fig. 3(a) Temperature variation *a*, *b* and *c* of $SmNbO_4$ compound

Fig. 3(b) Monoclinic angle (β) variation with temperature

Fig. 3(c) Variation of strain parameters ($(e_1 - e_2)^2, e_6{}^2$), volume ($V^{1/3}$) and basal area ($A^{1/2}$) with temperature

Fig. 4 Relation between spontaneous strain (e_s) and order parameter (η) of $SmNbO_4$ compound (solid spheres represents e_s values whereas solid line represents the order parameter)

Fig. 5(a) X-ray diffractograms of $SmNb_{1-x}(Si_{1/2}Mo_{1/2})_xO_4$ compositions

Fig. 5(b) Rietveld refinement plot of $SmNb_{0.31}(Si_{1/2}Mo_{1/2})_{0.69}O_4$ composition with tetragonal Scheelite structure

Fig. 5(c) Variation in lattice parameters of $SmNb_{1-x}(Si_{1/2}Mo_{1/2})_xO_4$ compositions

Fig. 6(a) Room temperature Raman spectra of $SmNb_{1-x}(Si_{1/2}Mo_{1/2})_xO_4$ compositions

Fig. 6(b) Deconvoluted Raman spectrum of $SmNb_{0.31}(Si_{1/2}Mo_{1/2})_{0.69}O_4$ composition

Fig. 7 Differential Scanning Calorimetry scan of $SmNb_{1-x}(Si_{1/2}Mo_{1/2})_xO_4$ compositions

Fig. 8 Surface morphology of $SmNb_{1-x}(Si_{1/2}Mo_{1/2})_xO_4$ compositions

(i) $SmNbO_4$ sintered at 1300 ^oC (ii) $SmNb_{0.31}(Si_{1/2}Mo_{1/2})_{0.69}O_4$ sintered at 1350 ^oC

Fig. 9 Variation in dielectric constant of $SmNb_{1-x}(Si_{1/2}Mo_{1/2})_xO_4$ compositions

Fig. 10 Variation in quality factor and temperature coefficient of resonant frequency of $SmNb_{1-x}(Si_{1/2}Mo_{1/2})_xO_4$ compositions

Table 1Crystallographic parameters of ambient and high temperature structures of $SmNbO_4$ compound

Atom	***x***	***y***	***z***	**Occupancy**	**Bond length (Å)**
At 30 ^{o}C, Space group: I2/a					
Sm	0.25	0.619(31)	0	1.0	Sm – O1(×2) : 2.330 Sm – O2(×2) : 2.217 (×2) : 2.540 Nb – O1(×2) : 1.983 Nb – O2(×2) : 1.797 (×2) : 2.338
Nb	0.25	0.144(30)	0	1.0	
O1	0.923(23)	0.953(8)	0.233(24)	1.0	
O2	0.468(31)	0.213(8)	0.786(4)	1.0	
At 800 ^{o}C, Space group: $I4_1/a$					
Sm	0	0.25	0.625	1.0	Sm – O(×4) : 2.420 (×4) : 2.473 Nb – O(×4) : 1.853
Nb	0	0.25	0.125	1.0	
O	0.243(31)	0.078(32)	0.038(12)	1.0	

Table 2 Temperature variation lattice parameters (*a*, *b*, *c* andβ) of $SmNbO_4$

Temp.(^{o}C)	***a* (Å)**	***b* (Å)**	***c* (Å)**	**β (°)**	**Refinement parameters ($_{w}R_p$, R_p, χ^2)**
30	5.425	11.18	5.121	94.64	8.2%, 9%, 1.98
100	5.415	11.192	5.127	94.46	9.2%, 8.6, 2.05
300	5.409	11.210	5.142	93.99	8.8%, 9.3, 2.12
600	5.390	11.258	5.180	92.96	8.3%, 10.2, 2.23
700	5.374	11.274	5.203	92.36	10.3%, 9.8%, 2.45
750	5.364	11.282	5.221	91.96	9.3%, 10.5%, 2.38
800	5.298	11.324	5.298	90.00	7.8%, 8.7%, 2.05
850	5.285	11.330	5.285	90.00	8.1%, 8.4%, 2.15

Table 3 Temperature variation strain parameters ($(e_1 - e_2)^2, e_6{}^2$), basal area ($A^{1/2}$) and volume ($V^{1/3}$) of $SmNbO_4$ compound

Temp.(^oC)	$(e_1 - e_2)^2$ **×10^{-3}**	$e_6{}^2$ **×10^{-3}**	**$A^{1/2}$ (Å)**	**$V^{1/3}$ (Å)**
30	3.326	6.54	5.262	6.764
100	2.98761	6.05	5.261	6.766
300	2.56315	4.84	5.267	6.775
600	1.5795	2.67	5.28	6.796
700	1.04578	1.69	5.286	6.804
750	0.73018	1.16	5.29	6.809
800	0	0	5.298	6.824
850	0	0	5.285	6.814

Table 4 Spontaneous strain values of $SmNbO_4$

Temp.(°C)	**u (×10^{-2})**	**v (×10^{-2})**	**e_s (×10^{-2})**
30	3.03	3.91	6.99
100	2.86	3.76	6.68
300	2.63	3.38	6.06
600	2.05	2.52	4.59
700	1.65	2.02	3.69
750	1.38	1.68	3.07
800	0	0	0

Table 5 Wyckoff sites, atomic coordinates and occupancies of $SmNb_{0.31}(Si_{1/2}Mo_{1/2})_{0.69}O_4$ composition

Atom	**Wyckoff site**	***x***	***y***	***z***	**Occupancy**
Sm	4b	0	0.25	0.625	1.0
Nb	4a	0	0.25	0.125	0.31
Si	4a	0	0.25	0.125	0.345
Mo	4a	0	0.25	0.125	0.345
O	16*f*	0.227(2)	0.081(2)	0.042(7)	1.0

Table 6. Raman mode assignment for $SmNb_{0.31}(Si_{1/2}Mo_{1/2})_{0.69}O_4$ composition

Mode	**Wave number (cm^{-1})**
A_g	884.4
B_g	814.4
E_g	765.7
-	657.4
-	524.1
B_g	446.6
A_g	415.8
E_g	362.9
A_g	337.0
B_g	233.0
-	216.6
-	176.6
-	146.1
E_g	117.1
B_g	100.0
-	67.60

Table 7 Lattice parameters, Percentage of theoretical density (ρ %) and microwave dielectric properties (dielectric constant (ε_r), quality factor (Q×*f*) and temperature coefficient of resonant frequency (τ_f)) of $SmNb_{1-x}(Si_{1/2}Mo_{1/2})_xO_4$ compositions

x	***a* (Å)**	***b* (Å)**	***c* (Å)**	***β* (º)**	**ρ (%)**	**ε_r**	**(Q×*f*) (GHz)**	**τ_f (ppm/ºC)**
0.0	5.425	11.192	5.127	94.75	95.6	17.3	48200	-47.3
0.03	5.423	11.182	5.122	94.65	94.7	17.1	46150	-46.1
0.04	5.420	11.178	5.120	94.60	94.2	16.8	45300	-45.6
0.68	5.157	5.157	11.378	90	95.4	15.9	33400	-39.6
0.69	5.158	5.158	11.38	90	93.8	15.6	32800	-38.2

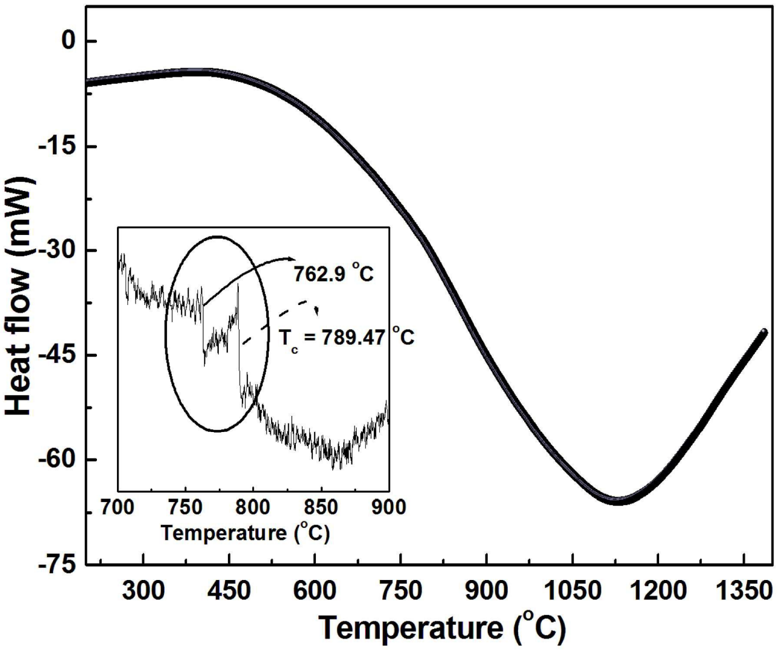

Fig. 1(a) Differential Scanning Calorimetry Scan of $SmNbO_4$ compound

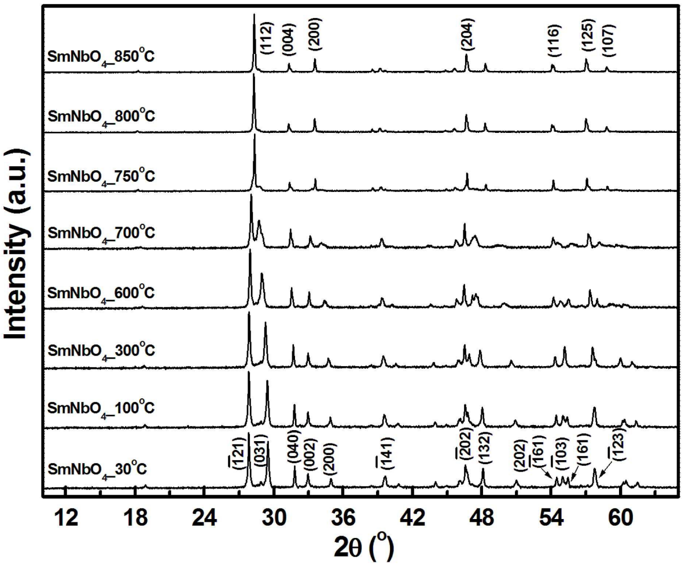

Fig. 1(b) Temperature variation X-ray diffractograms of $SmNbO_4$

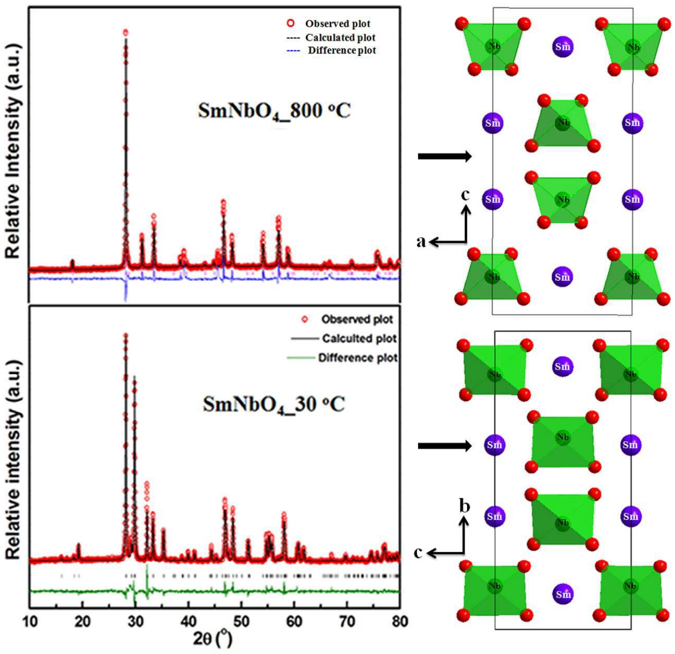

Fig. 2 (a) Rietveld refinement plots and crystal structure of SmNbO$_4$ at 30 °C and 800 °C

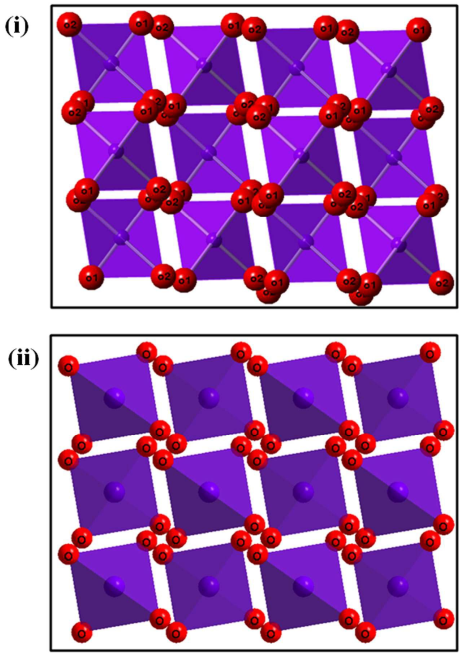

Fig. 2(b) Tetrahedral arrangement in (i) room temperature monoclinic fergusonite (ii) high temperature tetragonal scheelite structure

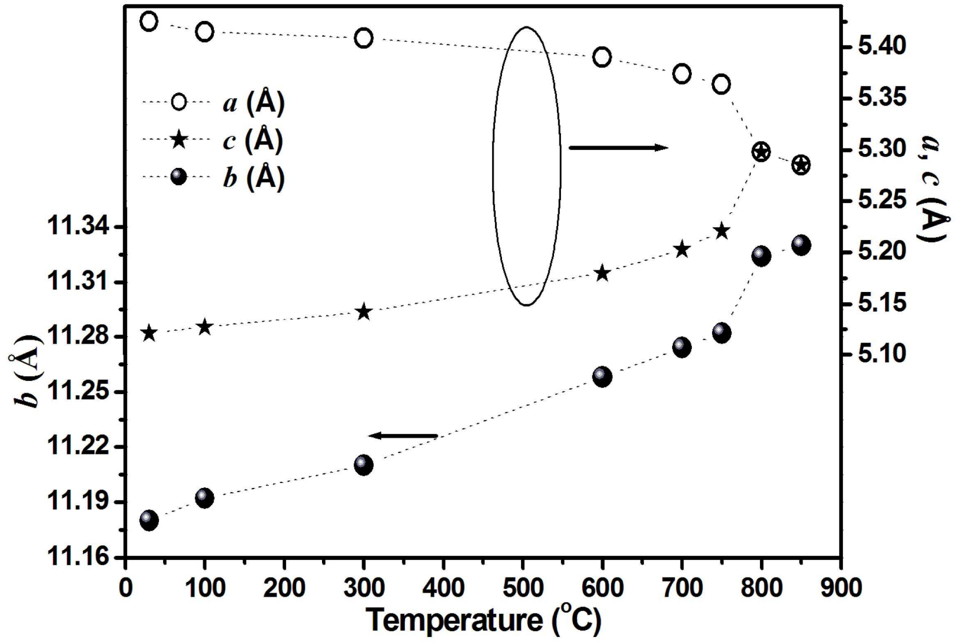

Fig. 3(a) Temperature variation *a*, *b* and *c* of $SmNbO_4$ compound

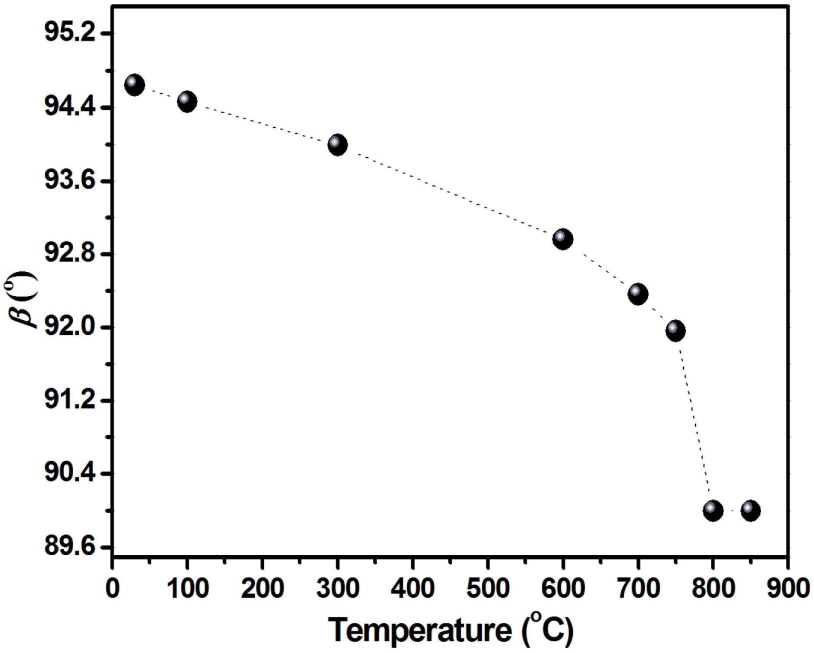

Fig. 3(b) Monoclinic angle (*β*) variation with temperature

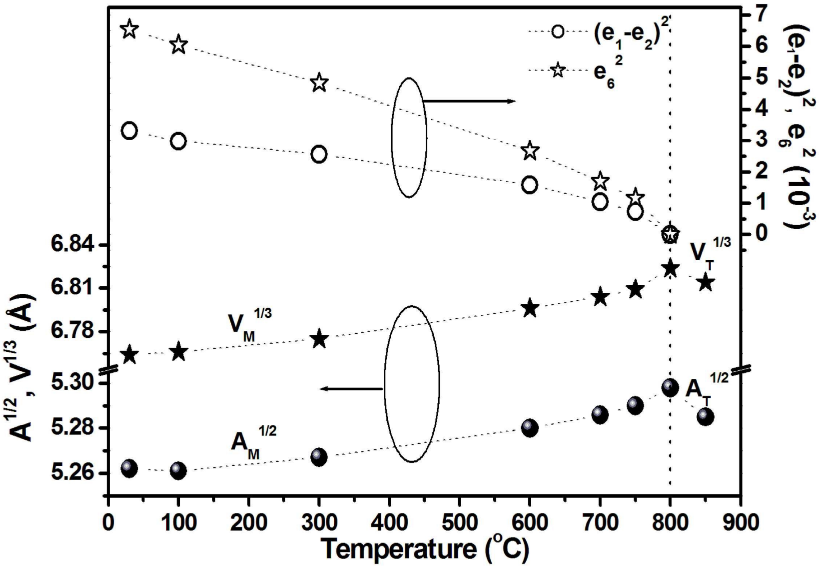

Fig. 3(c) Variation of strain parameters ($(e_1 - e_2)^2, e_6^2$), volume ($V^{1/3}$) and basal area ($A^{1/2}$) with temperature

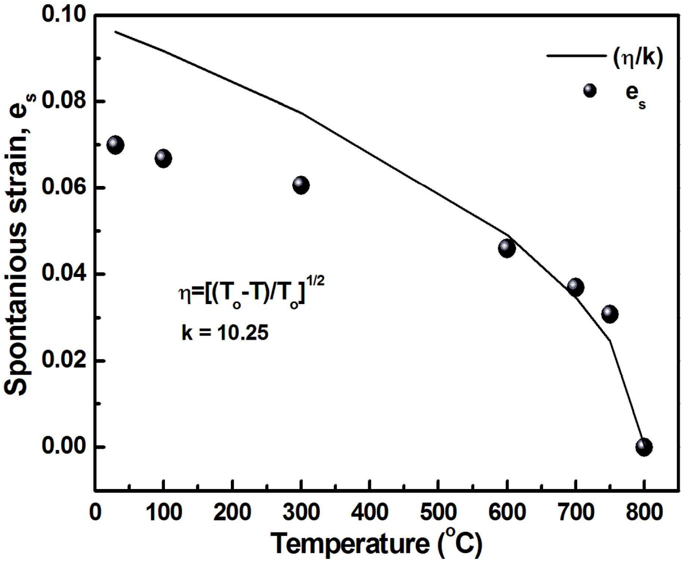

Fig. 4 Relation between spontaneous strain (e_s) and order parameter (η) of $SmNbO_4$ compound (solid spheres represents e_s values whereas solid line represents the order parameter)

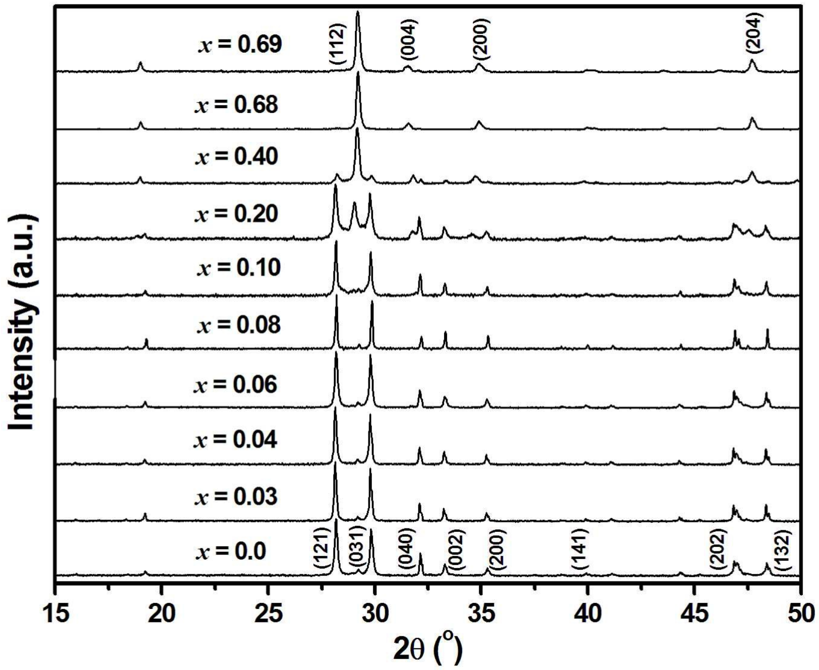

Fig. 5(a) X-ray diffractograms of $SmNb_{1-x}(Si_{1/2}Mo_{1/2})_xO_4$ compositions

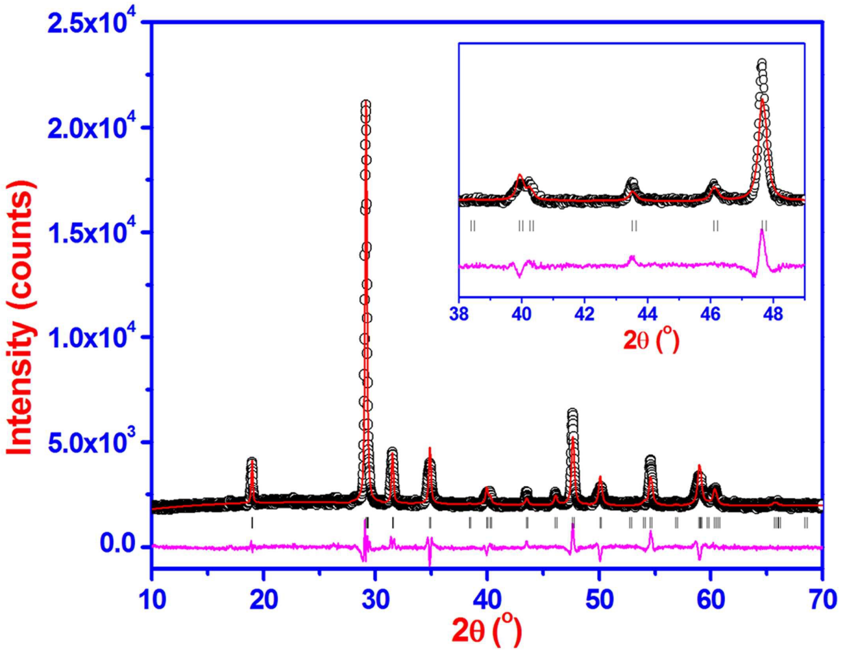

Fig. 5(b) Rietveld refinement plot of $SmNb_{0.31}(Si_{1/2}Mo_{1/2})_{0.69}O_4$ composition with tetragonal Scheelite structure

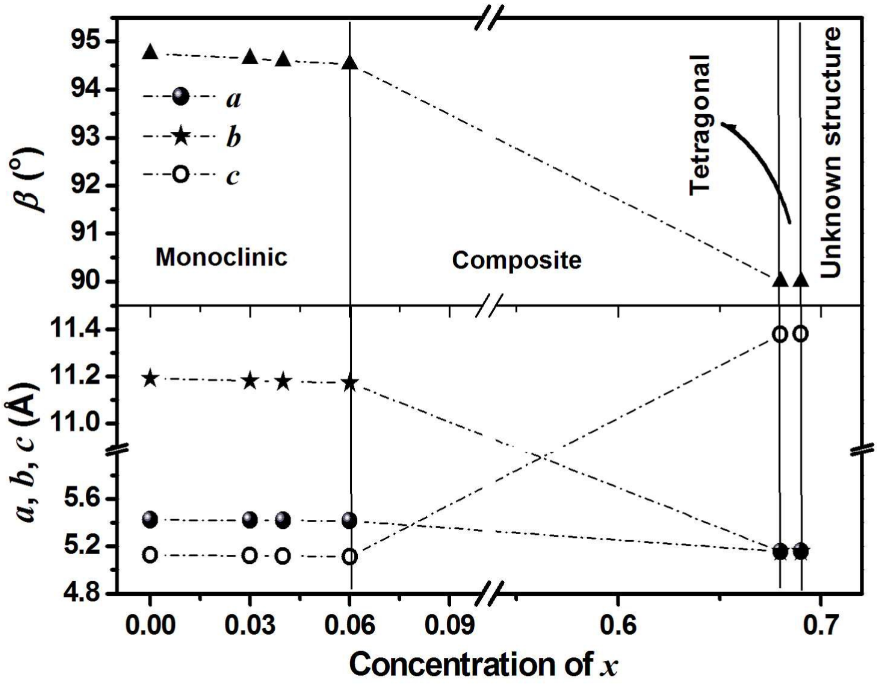

Fig. 5(c) Variation in lattice parameters of $SmNb_{1-x}(Si_{1/2}Mo_{1/2})_xO_4$ compositions

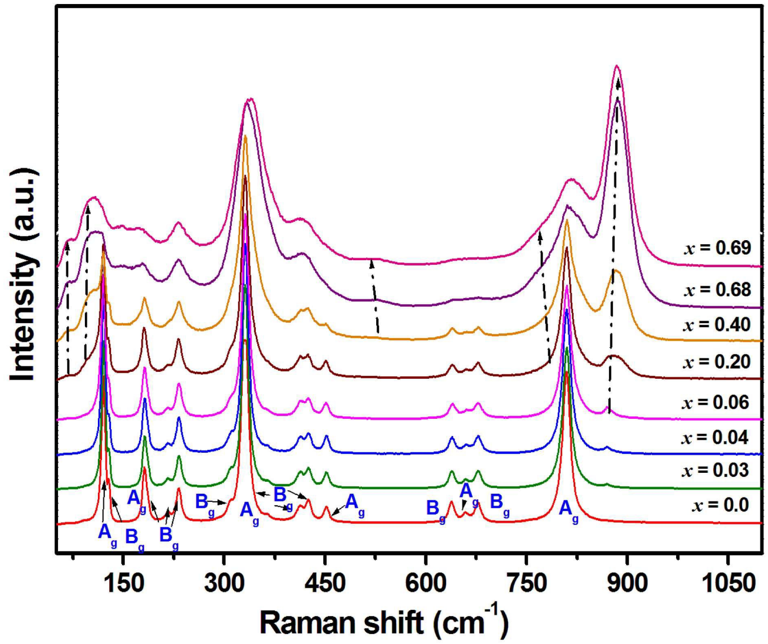

Fig. 6(a) Room temperature Raman spectra of $SmNb_{1-x}(Si_{1/2}Mo_{1/2})_xO_4$ compositions

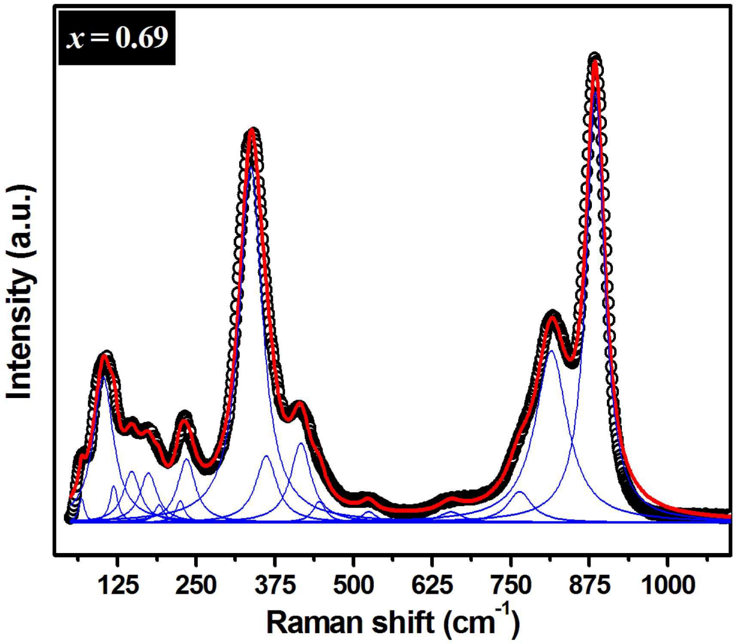

Fig. 6(b) Deconvoluted Raman spectrum of $SmNb_{0.31}(Si_{1/2}Mo_{1/2})_{0.69}O_4$ composition

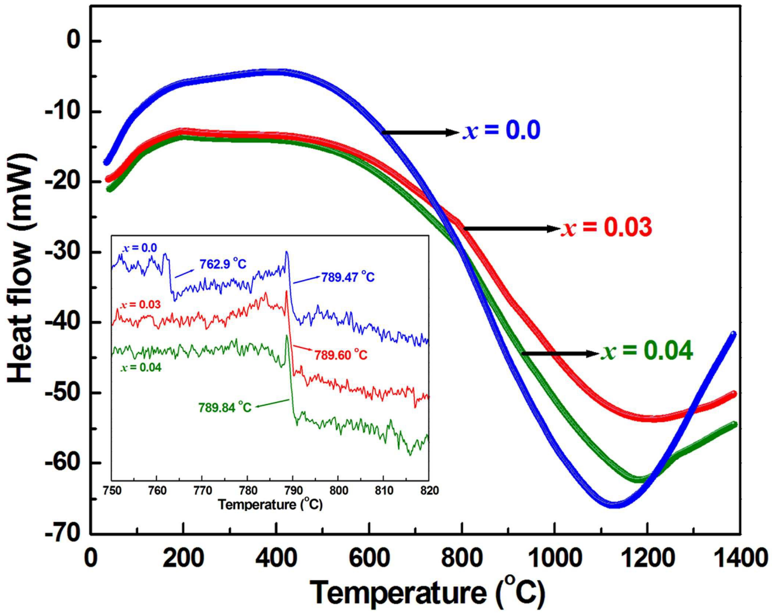

Fig. 7 Differential Scanning Calorimetry scan of $SmNb_{1-x}(Si_{1/2}Mo_{1/2})_xO_4$ compositions

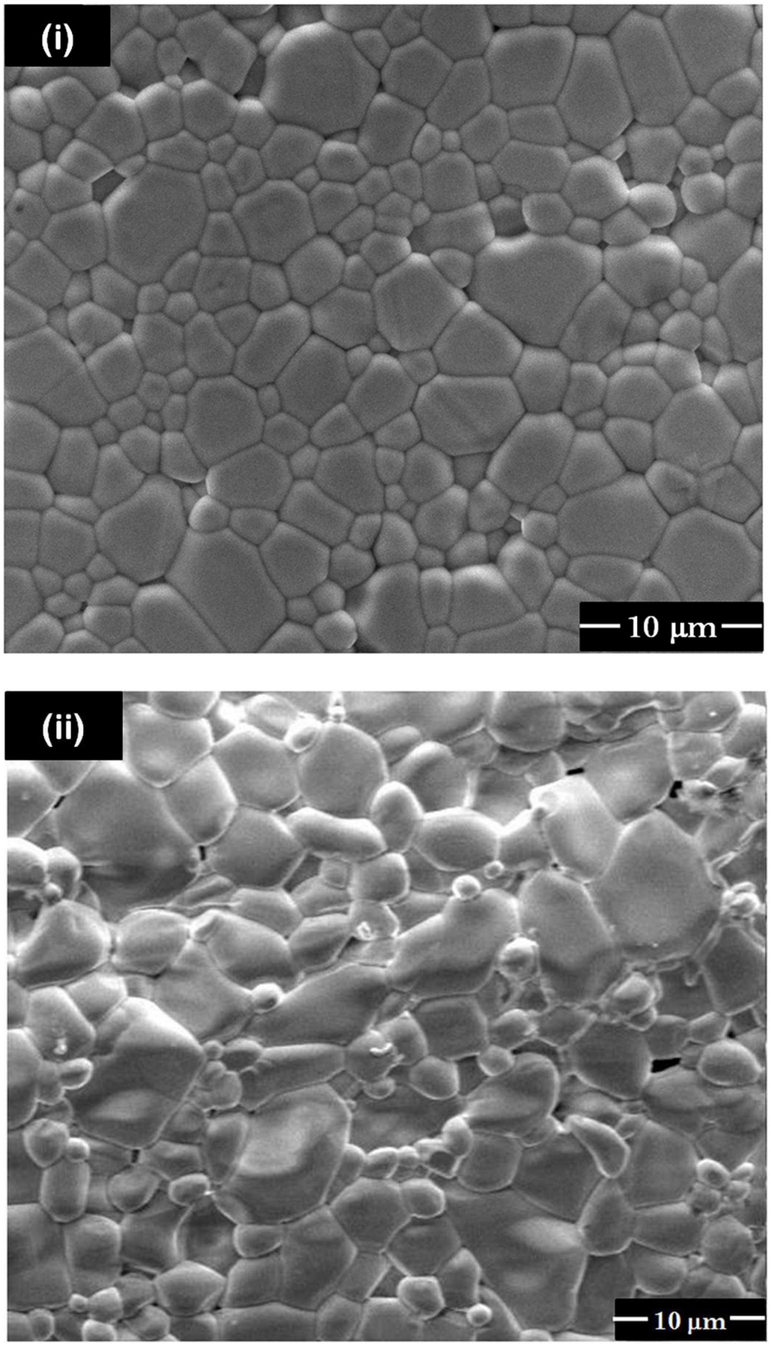

Fig. 8 Surface morphology of $SmNb_{1-x}(Si_{1/2}Mo_{1/2})_xO_4$ compositions

(i) $SmNbO_4$ sintered at 1300 °C (ii) $SmNb_{0.31}(Si_{1/2}Mo_{1/2})_{0.69}O_4$ sintered at 1350 °C

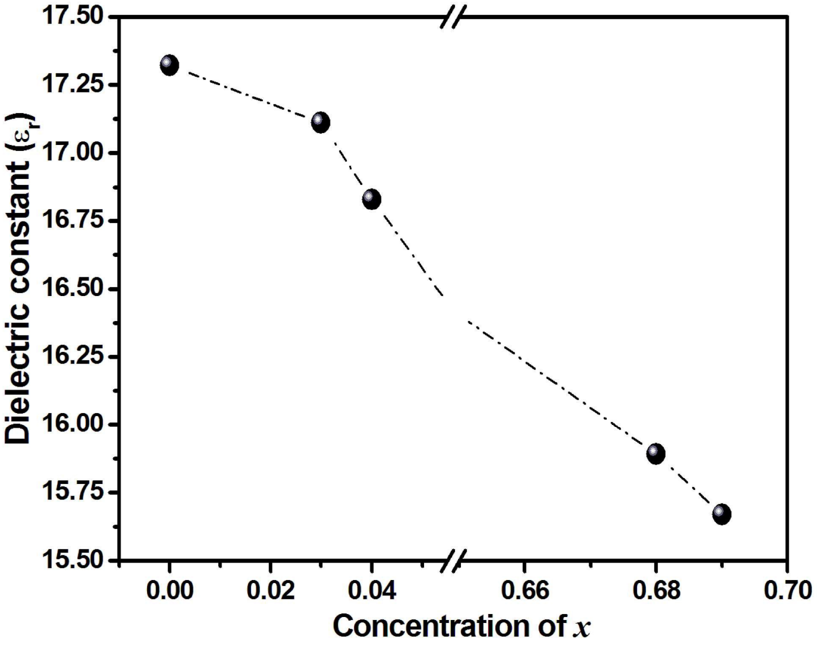

Fig. 9 Variation in dielectric constant of $SmNb_{1-x}(Si_{1/2}Mo_{1/2})_xO_4$ compositions

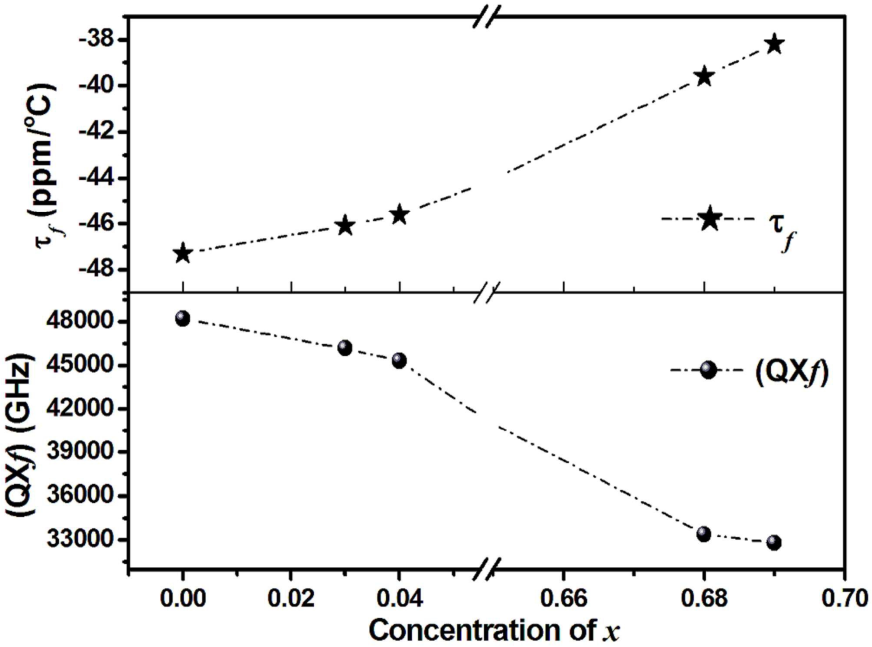

Fig. 10 Variation in quality factor and temperature coefficient of resonant frequency of

$SmNb_{1-x}(Si_{1/2}Mo_{1/2})_xO_4$ compositions